# Degradation and deactivation of a plasmid-encoded extracellular antibiotic resistance gene during separate and combined exposures to UV254 and radicals

Maolida Nihemaiti, Younggun Yoon, Huan He, Michael C. Dodd, Jean-Philippe Croué, Yunho Lee

# Degradation and deactivation of a plasmid-encoded extracellular antibiotic resistance gene during separate and combined exposures to $UV_{254}$ and radicals

Maolida Nihemaiti [a, 1], Younggun Yoon [b, 1], Huan He [c], Michael C. Dodd [c], Jean-Philippe Croué [a, d, *], and Yunho Lee [b, *]

[a] Curtin Water Quality Research Centre, Department of Chemistry, Curtin University, GPO Box U1987, Perth 6845, Australia

[b] School of Earth Sciences and Environmental Engineering, Gwangju Institute of Science and Technology (GIST), Gwangju 61005, Republic of Korea

[c] Department of Civil and Environmental Engineering, University of Washington, Seattle, Washington 98195-2700, United States

[d] Institut de Chimie des Milieux et des Materiaux IC2MP UMR 7285 CNRS, Universite de Poitiers, France

[1] M. Nihemaiti and Y. Yoon contributed equally to this work

*Corresponding authors: Yunho Lee, Email: yhlee42@gist.ac.kr

Jean-Philippe Croué, Email: jean.philippe.croue@univ-poitiers.fr

**Submitted to Water Research**

## Abstract

This study investigated the degradation and deactivation of an extracellular ampicillin resistance gene (*amp*$^R$) encoded in plasmid pUC19 during exposure to $UV_{254}$, •OH (generated by $UV_{>290}/H_2O_2$), and combined exposure to $UV_{254}$ and •OH ($SO_4^{\bullet-}$) using $UV_{254}/H_2O_2$ and $UV_{254}/S_2O_8^{2-}$. The degradation rates of *amp*$^R$ measured by quantitative polymerase chain reaction increased with increasing target amplicon length (192–851 bps). The rate constants for the degradation of pUC19 (2686 bps) were calculated as 0.26 $cm^2$/mJ for $UV_{254}$ and $1.5\times10^{11}$ $M^{-1}s^{-1}$ for •OH, based on the degradation rates of *amp*$^R$ amplicons and assuming an equal sensitivity of DNA damage across the entire plasmid. DNA repair-proficient *Escherichia coli (E. coli)* AB1157 strain (wild-type) and its repair-deficient mutants including AB1886 (*uvrA*$^-$), AB2463 (*recA*$^-$), AB2480 (*uvrA*$^-$, *recA*$^-$), and DH5α (*recA*$^-$, *endA*$^-$) were applied as recipient cells in gene transformation assays. Results suggested that the elimination efficiency of transforming activity during $UV_{254}$ and •OH exposure was dependent on the type of DNA repair genes in recipient *E. coli* strains. Losses of transforming activity were slower than the degradation of pUC19 by a factor of up to ~5 (for *E. coli* DH5α), highlighting the importance of DNA repair in recipient cell. The degradation rates of *amp*$^R$ amplicons were much larger (by a factor of ~4) in $UV_{254}/H_2O_2$ and $UV_{254}/S_2O_8^{2-}$ than $UV_{254}$ direct photolysis, indicating the significant contribution of •OH and $SO_4^{\bullet-}$ to the gene degradation. Not only $UV_{254}$ and $SO_4^{\bullet-}$, but also •OH contributed to the degradation of *amp*$^R$ during $UV_{254}/S_2O_8^{2-}$, which was attributed to the conversion of $SO_4^{\bullet-}$ to •OH and a 10-fold larger reactivity of •OH towards *amp*$^R$ as compared to $SO_4^{\bullet-}$. However, the enhanced gene degradation by radicals did not lead to a faster elimination of gene transforming activity during $UV_{254}/H_2O_2$ and $UV_{254}/S_2O_8^{2-}$, suggesting that $UV_{254}$- and radical-induced DNA damage were not additive in their contributions to losses of gene transforming activity. Wastewater effluent organic matter (EfOM) accelerated the degradation of *amp*$^R$ during $UV_{254}$ irradiation by means of reactive species production through

indirect photolysis reactions, whereas EfOM mainly acted as a radical scavenger during $UV_{254}/H_2O_2$ and $UV_{254}/S_2O_8^{2-}$ treatments.


## Keywords

Antibiotic resistant bacteria, antibiotic resistance genes, gene transformation, UV, hydroxyl radical, sulfate radical

## Abbreviations

| | |
|---|---|
| $amp^R$ | Ampicillin Resistance Gene |
| AOPs | Advanced Oxidation Processes |
| Amp | Amplicon |
| ARB | Antibiotic Resistant Bacteria |
| ARG(s) | Antibiotic Resistance Gene(s) |
| bp(s) | Nucleotide Base Pair(s) |
| DOM | Dissolved Organic Matter |
| e-ARG | Extracellular Antibiotic Resistance Genes |
| *E. coli* | *Escherichia coli* |
| EfOM | Effluent Organic Matter |
| *p*CBA | *para*-Chlorobenzoic Acid |
| qPCR | Quantitative Polymerase Chain Reaction |

# 1. Introduction

Antibiotic resistance is a natural phenomenon. However, anthropogenic activities (e.g., overuse and disposal of antibiotics) are providing constant selection pressure on antibiotic resistant bacteria (ARB) (Vikesland, Pruden et al. 2017). Antibiotic resistance can be developed and disseminated within the bacterial population by genetic mutation, cell division, and the transfer of antibiotic resistance genes (ARGs) (Davies and Davies 2010). ARGs are contaminants of concern in natural and engineered aquatic systems, as ARG transfer can be linked with the spread of antibiotic resistance to human pathogens (Dodd 2012, Pruden 2014). Mobile genetic elements carrying ARGs (e.g., plasmids, integrons, and transposons) can be disseminated to and expressed by recipient cells through horizontal gene transfer (HGT), including conjugation (mediated by cell to cell contact), transduction (bacteriophage mediated), and transformation (mediated by extracellular DNA) (Lorenz and Wackernagel 1994) Of these, transformation can be understood to represent the most basic mode of HGT, as it does not require the presence of live donor cells or bacteriophages (Lorenz and Wackernagel 1994). Consequently, quantification of the frequency with which an ARG in extracellular DNA can be transported into and expressed by a recipient cell through transformation (hereafter referred to as *transforming activity*) can provide a conservative measure of the ability of an ARG to undergo HGT. Transforming activity encompasses (a) efficiency of extracellular DNA transport into a recipient cell, (b) any repair of that DNA by the recipient cell in the event the DNA is damaged, and (c) heritable incorporation and expression of the DNA's genetic information by recipient cells, and is therefore a function of both the recipient cell's ability to import, repair, and express a given ARG and the quality and quantity of the extracellular DNA containing the ARG. Extracellular DNA can be released into the environment though secretion by live cells and lysis of dead cells. While unstable to nucleases likely to be present in many aquatic matrixes, it can

85 persist in the environment through adsorption onto soil and sediments (Lorenz and Wackernagel
86 1994, Mao, Luo et al. 2014, Nagler, Insam et al. 2018).

87 Although conventional disinfection processes during water treatment (e.g., chlorine and UV)
88 efficiently inactivate ARB, intracellular ARGs are more difficult to degrade (McKinney and
89 Pruden 2012, Yoon, Chung et al. 2017, He, Zhou et al. 2019) and can be released into water
90 following the death of ARB cells (Zheng, Su et al. 2017). Sub-inhibitory concentrations of
91 disinfectants (e.g., chlorine and monochloramine) were even reported to promote the horizontal
92 transfer of ARGs by increasing the permeability of cell membrane and altering the expression of
93 conjugation-related genes (Guo, Yuan et al. 2015, Zhang, Gu et al. 2017). The proportion of
94 extracellular DNA carrying ARGs was found to increase after various biological and chemical
95 processes in wastewater treatment, revealing the potential risk of antibiotic resistance
96 dissemination in discharged effluent and receiving environments (Liu, Qu et al. 2018, Zhang, Li
97 et al. 2018). Previous studies have reported the enrichment of ARGs in surface water due to the
98 discharged effluents from upstream wastewater plants (Cacace, Fatta-Kassinos et al. 2019, Wu,
99 Su et al. 2019, Osińska, Korzeniewska et al. 2020). High diversity of ARGs in reclaimed
100 wastewater (e.g., agriculture irrigation, potable reuse) may pose risks of antibiotic resistance
101 dissemination to environmental bacteria and even human pathogens (Christou, Agüera et al.
102 2017, Hong, Julian et al. 2018).

103 UV-based advanced oxidation processes (UV-AOPs) are increasingly applied for the removal
104 of refractory contaminants during water treatment. The elimination of contaminants in UV-AOP
105 treatment is achieved by dual pathways, namely direct UV photolysis (depending on the UV
106 absorbances and quantum yields of target compounds) and oxidation by powerful radical species
107 (Stefan 2018). The activation of hydrogen peroxide ($UV/H_2O_2$) and peroxydisulfate ($UV/S_2O_8^{2-}$)
108 by UV light produces hydroxyl radical (•OH) and sulfate radical ($SO_4^{\bullet-}$), respectively, which
109 can degrade a wide range of contaminants, as these two radicals react with many compounds at

or near diffusion-controlled reaction rates (Buxton, Greenstock et al. 1988, Neta, Huie et al. 1988).

$UV/H_2O_2$ and $UV/S_2O_8^{2-}$ have also been reported to efficiently inactivate ARB cells (Michael-Kordatou, Iacovou et al. 2015, Ferro, Guarino et al. 2016, Giannakis, Le et al. 2018). However, detailed investigation into the reactivity of •OH with intracellular ARGs in these studies was limited due to the significant consumption of •OH by constituents of the water matrix and cell membranes before reaching the cell interiors (Ferro, Guarino et al. 2017, Yoon, Chung et al. 2017, Zhang, Hu et al. 2019). Recent studies have reported that the reactivity of •OH with extracellular chromosomal ARGs is highly dependent on the length of the monitored ARG targets (He, Zhou et al. 2019). More studies are needed to assess whether the observed reactivities are generally applicable to other types of DNA such as plasmid-encoded ARGs. To the best of the authors' knowledge, little is known on the fate of ARGs during $SO_4^{\bullet-}$-based treatment processes.

Quantitative polymerase chain reaction (qPCR) has been widely applied to quantify structurally-intact ARGs or to measure their degradation rates in water and wastewater treatment (McKinney and Pruden 2012, Luby, Ibekwe et al. 2016, Hiller, Hübner et al. 2019). It should be noted that qPCR methods usually record the degradation of a small fraction of a target ARG's sequence length (with amplicon sizes typically <1000 bps), and not the entirety of a gene (McKinney and Pruden 2012, Chang, Juhrend et al. 2017, Yoon, Dodd et al. 2018). In addition, the efficiency of DNA replication (particularly of damaged DNA) in qPCR methods can be different from that observed in bacterial cells subjected to transformation with the same DNA. Furthermore, the uptake and repair of DNA by recipient cells can play important roles in modulating gene transforming activity (Chang, Juhrend et al. 2017, Yoon, Dodd et al. 2018). While the correlation between the degradation of target ARG amplicons (measured by qPCR)

and the elimination of ARG transforming activity was reasonably well explained for chromosomal ARGs (He, Zhou et al. 2019), it is still less clear for plasmid-borne ARGs.

Exposure of DNA to UV and •OH is known to induce different types of DNA damage (von Sonntag 2006). UV-C generates cyclobutane-pyrimidine dimers (CPDs) as the predominant DNA lesions, while •OH can induce DNA damage ranging from base oxidation to phosphate-sugar backbone breakages (Görner 1994, Sinha and Häder 2002, von Sonntag 2006). It is currently not completely clear how the various type(s) of DNA damage resulting from UV, •OH, and $SO_4^{\bullet-}$ are related to the deactivation of ARGs; for example, whether DNA lesions such as CPDs (formed by direct UV irradiation) have the same effect on DNA transforming activity as phosphate-sugar backbone breakage by •OH (generated by $H_2O_2$ or $S_2O_8^{2-}$ photolysis). Furthermore, in UV-AOPs, DNA lesions can be generated by both direct UV irradiation and radicals simultaneously.

The aim of this study was to investigate the fate of plasmid-encoded e-ARGs during the common UV at 254 nm water disinfection process ($UV_{254}$) and its related AOPs. Plasmid (pUC19) encoding an ampicillin resistance gene (*amp*$^R$) was purified from *Escherichia coli* (*E. coli*) host cells and exposed to $UV_{254}$, to $UV_{254}$ in combination with •OH or $SO_4^{\bullet-}$ (by using $UV_{254}/H_2O_2$ and $UV_{254}/S_2O_8^{2-}$), or to •OH only (by combining UV at >290 nm with $H_2O_2$) (i.e., $UV_{>290}/H_2O_2$). $UV_{>290}/H_2O_2$ treatment was chosen to study the effect of •OH only exposure because irradiation of $H_2O_2$ by $UV_{>290}$ can generate •OH, while neither $UV_{>290}$ irradiation nor $H_2O_2$ directly affect *amp*$^R$ under these experimental conditions (detailed in Section 3.1). The treated plasmid samples were analysed by qPCR, gel electrophoresis, and ARG transformation assay. DNA repair-proficient *E. coli* AB1157 (wild-type), as well as repair-deficient *E. coli* mutants including AB1886 (*uvrA*$^-$), AB2463 (*recA*$^-$), AB2480 (*uvrA*$^-$, *recA*$^-$), and DH5α (*recA*$^-$, *endA*$^-$) were employed as recipient cells in the ARG transformation assay. Competition kinetics methods using radical probe compounds were applied to measure the second-order rate

159 constants of •OH and $SO_4^{\bullet-}$ with $amp^R$ segments. Experiments were also conducted in the
160 presence of wastewater effluent organic matter (EfOM) to study the effect of the dissolved
161 organic matter (DOM) on the removal of e-ARGs.

## 162 2. Materials and Methods

### 163 2.1 Chemical Reagents

164 All chemicals were in analytical grade or higher and used as received without further
165 purification. Ampicillin sodium salt (#A0166), agar powder (#A1296), sodium chloride
166 (≥99.5%), *para*-chlorobenzoic acid (99%), and nitrobenzene (≥99%) were purchased from
167 Sigma-Aldrich. Tryptone (#1612) and yeast extract (#1702) were supplied from Laboratorios
168 CONDA. Hydrogen peroxide 30% (Thermo Fisher Scientific) and sodium peroxydisulfate
169 (≥98%, Sigma-Aldrich) were used to prepare the stock solutions of $H_2O_2$ and $S_2O_8^{2-}$,
170 respectively. All solutions were prepared in Milli-Q water (18 MΩ·cm, Millipore). EfOM was
171 previously extracted from the discharged effluent of a wastewater treatment plant in Jeddah,
172 Saudi-Arabia, with XAD resins (Zheng, Khan et al. 2014). Solutions of EfOM were prepared by
173 dissolving the hydrophobic and transphilic fractions (2:1 by mass) of EfOM in phosphate buffer.

### 174 2.2 Plasmid Preparation

175 Plasmid pUC19 was extracted from *E. coli* DH5α. pUC19 (2686 bp) is a commercially
176 available *E. coli* vector carrying an ampicillin resistance gene ($amp^R$, 861 bp). One hundred μL
177 of *E. coli* DH5α mid-exponential growth phase culture in LB broth medium with 50 mg/L of
178 ampicillin was transferred into 150 mL of LB broth medium containing 50 mg/L of ampicillin
179 and incubated overnight (200 rpm, 37°C). Plasmids were extracted from this overnight stock
180 solution using an AccuPrep Plasmid Mini Extraction kit (Bioneer 2016). The concentration of
181 recovered plasmid DNA was measured on a NanoDrop ND-2000 Spectrophotometer
182 (NanoDrop Products, Wilmington, USA).

183 **2.3 UV Experiments**

184 $UV_{254}$-based experiments were carried out with a UV quasi-collimated beam device equipped
185 with a low-pressure mercury lamp emitting UV light primarily at 254 nm (Sankyo Denki Ltd.,
186 Tokyo, Japan). The UV light was collimated onto the experimental solution, which was
187 contained in a petri dish placed on a magnetic stirrer. The average UV intensity (0.3 $mW/cm^2$)
188 was determined with atrazine chemical actinometry (Lee, Gerrity et al. 2016). Experimental
189 solutions were prepared in autoclaved 2 mM phosphate buffer at pH 7. The initial concentration
190 of plasmid DNA used in experiments was 0.3 or 1 µg/mL. The applied UV fluences ranged from
191 0−180 $mJ/cm^2$. The initial concentrations of $H_2O_2$ and $S_2O_8^{2-}$ were 0.5 mM for $UV_{254}/H_2O_2$ and
192 $UV_{254}/S_2O_8^{2-}$, respectively. $UV_{>290}/H_2O_2$ experiments were conducted using a Model 66924 arc
193 lamp source fitted with a 450-W $O_3$-free Xe arc lamp and focusing collimator, and equipped
194 with an atmospheric attenuation filter and dichroic mirror to restrict lamp output to near-UV
195 wavelengths (290 nm < λ < 400 nm) (Newport-Oriel Model 66924; Stratford, CT). Relatively
196 high $H_2O_2$ concentrations (i.e., 10 mM) were applied for $UV_{>290}/H_2O_2$, in order to increase the
197 yield of •OH due to the low absorbance of UV light by $H_2O_2$ in this wavelength region. Samples
198 were withdrawn from the irradiated solutions in each experimental setup at predetermined time
199 intervals for DNA and probe compound analyses. Residual $H_2O_2$ and $S_2O_8^{2-}$ were quenched
200 with excess bovine catalase and sodium thiosulfate, respectively. Samples for DNA analysis
201 (500 µL) were stored at -20°C and analysed within 24 h. Control experiments indicated that
202 $H_2O_2$ and $S_2O_8^{2-}$ did not affect qPCR analyses within these experimental conditions (Figure S1).

203 **2.4 Radical probe compounds**

204 *para*-chlorobenzoic acid (*p*CBA) was used as •OH probe during $UV_{254}/H_2O_2$ and
205 $UV_{>290}/H_2O_2$ experiments. Both *p*CBA and nitrobenzene were applied during $UV_{254}/S_2O_8^{2-}$.
206 Nitrobenzene can be used as a selective •OH probe compound ($k_{\bullet OH}$=3.9×10$^9$ $M^{-1}$ $s^{-1}$) (Buxton,

Greenstock et al. 1988) due to its low reactivity to $SO_4^{\bullet-}$ ($k_{SO_4^{\bullet-}}$<$10^6$ $M^{-1}$ $s^{-1}$) (Neta, Madhavan et al. 1977), whereas *p*CBA reacts with both radicals (i.e., $k_{SO_4^{\bullet-}}$=$3.6\times10^8$ $M^{-1}$ $s^{-1}$ and $k_{\bullet OH}$=$5\times10^9$ $M^{-1}$ $s^{-1}$) (Neta, Madhavan et al. 1977, Buxton, Greenstock et al. 1988). *p*CBA and nitrobenzene were analysed on a high-performance liquid chromatograph (HPLC, Dionex Ultimate 3000, Thermo Scientific) equipped with an XDB-C18 column (5 µm, 4.6 × 150 mm, Agilent). The mobile phase comprised acetonitrile and 10 mM phosphoric acid (40:60, v/v). The two probe compounds were analysed at their maximum absorbance wavelengths (i.e., 240 and 270 nm for *p*CBA and nitrobenzene, respectively).

### 2.5 qPCR Analysis

Gene degradation was measured by qPCR using a CFX96 real-time PCR detection system (Bio-Rad, Hercules, CA, USA). Four different amplicons (i.e., 192, 400, 603, and 851 bp) were monitored, which covered varying fractions of *amp*$^R$ as shown in Figure S2. The longest size of *amp*$^R$ segment targeted in qPCR was 851 bp instead of the whole *amp*$^R$ gene (861 bp), due to the low amplification efficiency of the 861 bp amplicon in the qPCR method. The reaction mixture (20 µL) consisted of 1 µL of each primer, 1 µL of sample, 10 µL of EvaGreen® supermix, and 7 µL of autoclaved DNase free water. The qPCR protocol included one cycle at 95°C for 2 min, 30 cycles at 95°C for 5 s, an annealing step at 55°C for 60 s, and an elongation at 72°C for 20 s, followed by a melt curve analysis from 65°C to 95°C. Each sample was analysed in triplicate. More information on qPCR analysis, the DNA sequence of *amp*$^R$, and the monitored qPCR target amplicons is described elsewhere (Yoon, Dodd et al. 2018).

### 2.6 Gel Electrophoresis Analysis

pUC19 plasmid (1 µg/mL) treated by $UV_{254}$ and •OH ($UV_{>290}/H_2O_2$) was analysed by gel electrophoresis to investigate the structural change of plasmid DNA. Linearized pUC19 was also prepared for a reference by incubating the plasmid with type II restriction enzyme *EcoRI* (NEB,

231 USA) at 37 °C for 1 h, followed by enzyme inactivation at 65°C for 20 min. Plasmid samples
232 from $UV_{254}$, •OH ($UV_{>290}/H_2O_2$), and enzyme treatments, as well as a 1 kb DNA ladder
233 (Enzynomics, Korea) were loaded on 0.8% agarose gels at 4 V $cm^{-1}$ for 35 min. The bands were
234 visualized by ethidium bromide staining. Gel images were captured on a UV transilluminator
235 (Universal mutation detection system, UVP, LLC, USA).

236 **2.7 Gene Transformation Assays**

237 Non-ampicillin resistant *E.coli* K12 bacteria strains DH5α (*recA*$^-$, *endA*$^-$), AB1157 (wild-
238 type), AB1886 (*uvrA*$^-$), AB2463 (*recA*$^-$), and AB2480 (*uvrA*$^-$, *recA*$^-$) were used as recipient
239 cells for gene transformation assays. DH5α strain was commercially available from ATCC;
240 others were provided by CGSC (Coli Genetic Stock Center at Yale University). Details on
241 transformation assays were described by Yoon, Dodd et al. (2018). In brief, competent cells
242 were prepared by chemical treatment of non-resistant *E. coli* K12 strains using calcium chloride
243 and glycerol (Shanehbandi, Saei et al. 2013) and preserved at -80°C until use. Fifty μL of
244 treated plasmid sample was mixed with 100 μL of thawed competent cells. After incubating in
245 ice for 30 min, the mixture was quickly transferred onto a digital test tube heater (45°C) for 45 s
246 and then placed back in ice for 2 min. After the heat shock, the samples were mixed with 900
247 μL of LB broth and cultured for 45 min (200 rpm, 37°C). Finally, the incubated samples were
248 serially diluted with LB broth and plated onto two types of LB agar plates (i.e., with and without
249 inclusion of 50 mg/L of ampicillin). After 24 h of incubation at 37°C, the number of ARB
250 colonies (transformants) detected on selective agar plates (with ampicillin) were compared with
251 the total recipient cells growing on nonselective agar plates (without ampicillin). The gene
252 transformation efficiency was calculated as follows:

253 $$\text{Transformation efficiency} = \frac{Transformant\ cells_{selective\ plate}\ (CFU/mL)}{Total\ recipient\ cells_{nonselective\ plate}\ (CFU/mL)}$$

The typical concentrations of total recipient cells, as measured by culturing on nonselective agar plates (without ampicillin), were approximately $3\times10^8$ and $2\times10^8$ CFU/mL for *E. coli* DH5α and *E. coli* AB strains, respectively. Control experiments conducted by directly plating the recipient cells (without heat shock) on nonselective plates showed <10% variation in the final colony counts of recipient cells as compared to the conditions incorporating heat shock (Figure S3), and <50% variation in colony counts between strains. These results indicated that the type of bacterial strain used, or stresses to which the strains were subjected during transformation assays (e.g., heat shock), did not significantly impact the fitness or growth rates of recipient cells on nonselective plates. Calibration curves prepared with known concentrations of plasmid DNA indicated that the number of transformants linearly increased with increasing plasmid DNA concentration from $10^{-5}$–$10^{-1}$ μg/mL (Figure S4). The transformation efficiency of $amp^R$ calculated for *E. coli* K12 strains was in the range of $10^{-4}$ – $10^{-8}$, which was comparable with previous studies (Chang, Juhrend et al. 2017, Yoon, Dodd et al. 2018).

### 2.8 Statistical analysis

Statistical analysis was conducted using SigmaPlot 12.0 and GraphPad Prism 7.0. The fluence-based rate constants for gene degradation and transformation efficiency loss under various experimental conditions were compared by multiple linear regression analysis. The null hypothesis was that the first-order rate constants were identical, with $p$=0.05 as the threshold significance level.

## 3. Results and Discussions

### 3.1 e-ARG degradation during separate exposure to $UV_{254}$ and •OH

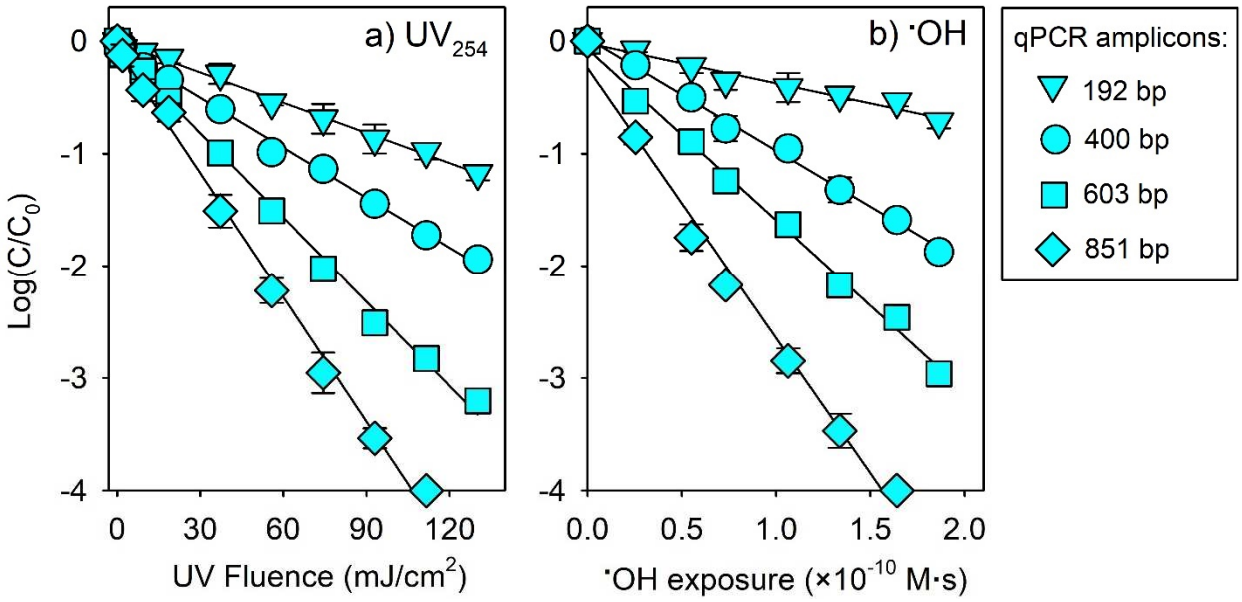


**Figure 1.** Degradation of *amp*$^R$ segments during the treatment of pUC19 (1 µg/mL) with (a) $UV_{254}$ and (b) •OH ($UV_{>290}/H_2O_2$) at pH 7 (2 mM phosphate buffer). 10 mM of $H_2O_2$ and 1 µM of *p*CBA were added in $UV_{>290}/H_2O_2$ experiments. Error bars represent the standard deviations of triplicate experiments. Lines are the linear regressions of the experimental data.

*$UV_{254}$ exposure (Figure 1a).* The solution containing pUC19 was irradiated with $UV_{254}$ light (0–130 mJ/cm$^2$). The degradation of *amp*$^R$ segments (192, 400, 603, and 851 bp) measured by qPCR followed first-order kinetics with respect to UV fluence ($r^2$ >0.99) (Figure 1a). The 192 bp *amp*$^R$ segment was degraded by about 1-log at 110 mJ/cm$^2$, whereas 4-log reduction was already achieved for the 851 bp segment, which was close to the overall size of *amp*$^R$ (861 bp). The resulting fluence-based rate constants derived from the slopes of linear curves, $k_{UV,Amp}$ = 2.303 × slope, are summarized in Table 1. The $k_{UV,Amp}$ of *amp*$^R$ segments increased with amplicon size, which was consistent with the increasing number of potential reaction sites with increasing number of nucleotide bps. The $k_{UV,Amp}$ values obtained from this study were comparable to previously-reported values for the same *amp*$^R$ segments (Yoon, Dodd et al. 2018). The $k_{UV,plasmid}$ of pUC19 plasmid could be estimated by extrapolating the $k_{UV,Amp}$ of each

segment to the entire plasmid (e.g., $k_{UV,plasmid}$=$k_{UV,192bp}$×$\frac{2686\ bp}{192\ bp}$), based on an assumption that the UV reactivity per base pair is the same across the entire plasmid. The $k_{UV,plasmid}$ values estimated from the 192, 400, 603, and 851 bp amplicons were 2.9(±0.06)×$10^{-1}$, 2.3(±0.04)×$10^{-1}$, 2.6(±0.05)×$10^{-1}$, and 2.7(±0.06)×$10^{-1}$ $cm^2$/mJ, respectively, yielding an average $k_{UV,plasmid}$ value of 2.6(±0.05)×$10^{-1}$ $cm^2$/mJ (Table 1).

A theoretical approach was recently employed to estimate the photoreactivity of DNA (i.e., formation rate of CPDs and 6,4-photoproducts) based on the molar absorption coefficients, quantum yields, and the number of 5'-bipyrimidine-3' doublets of a given DNA (Yoon, Dodd et al. 2018, He, Zhou et al. 2019). By applying this approach, the overall DNA lesion formation rate on pUC19 upon $UV_{254}$ exposure, $k_{all\ lesions}$, was calculated as 2.1×$10^{-1}$ $cm^2$/mJ (Text S1), which was close to the average $k_{UV,plasmid}$ (2.6×$10^{-1}$ $cm^2$/mJ) predicted from qPCR results as mentioned above.

**Table 1.** Apparent rate constants for the degradation of *amp*$^R$ segments and pUC19 plasmid, and the elimination of gene transforming activity during $UV_{254}$ and •OH only treatments [a]

| *amp*$^R$ segments | | pUC19 plasmid [b] | | Loss of gene transformation | |
|---|---|---|---|---|---|
| #base pairs (bps) | $k_{Amp}$ | $k_{plasmid}$ | average | Recipient cells | $k_{transformation}$ |
| $UV_{254}$ ($cm^2$/mJ) | | | | | |
| 192 | 2.0(±0.05)×$10^{-2}$ | 2.9(±0.06)×$10^{-1}$ | 2.6(±0.05)×$10^{-1}$ | DH5α | 6.5(±0.21)×$10^{-2}$ |
| 400 | 3.4(±0.07)×$10^{-2}$ | 2.3(±0.04)×$10^{-1}$ | | AB1157 | 1.0(±0.03)×$10^{-1}$ |
| 603 | 5.8(±0.11)×$10^{-2}$ | 2.6(±0.05)×$10^{-1}$ | | AB1886 | 2.4(±0.06)×$10^{-1}$ |
| 851 | 8.9(±0.16)×$10^{-2}$ | 2.7(±0.06)×$10^{-1}$ | | AB2463 | 1.6(±0.06)×$10^{-1}$ |
| •OH ($UV_{>290}$/$H_2O_2$) ($M^{-1}$ $s^{-1}$) | | | | | |
| 192 | 8.1(±0.69)×$10^9$ | 1.2(±0.10)×$10^{11}$ | 1.5(±0.07)×$10^{11}$ | DH5α | 2.7(±0.05)×$10^{10}$ |
| 400 | 2.2(±0.07)×$10^{10}$ | 1.5(±0.05)×$10^{11}$ | | AB1157 | 4.1(±0.14)×$10^{10}$ |
| 603 | 3.5(±0.10)×$10^{10}$ | 1.6(±0.04)×$10^{11}$ | | AB1886 | 6.5(±0.18)×$10^{10}$ |
| 851 | 5.6(±0.27)×$10^{10}$ | 1.8(±0.08)×$10^{11}$ | | AB2463 | 8.2(±0.23)×$10^{10}$ |

[a] Experimental conditions: pUC19: 1 μg/mL, 2 mM phosphate buffer at pH 7, fluence range for $UV_{254}$: 0–130 mJ/$cm^2$, 10 mM of $H_2O_2$ and 1 μM of *p*CBA were added in $UV_{>290}$/$H_2O_2$. The apparent rate constant values were reported in the form of Mean ± Standard Error.

[b] The $k_{plasmid}$ values of pUC19 plasmid were estimated based on the $k_{Amp}$ of *amp*$^R$

segments obtained from qPCR analyses (see Section 3.1 for details).

*•OH exposure (Figure 1b).* Control experiments have confirmed that *amp*$^R$ segments were stable under $UV_{>290}$ irradiation alone (Figure S5), which was attributed to the low UV absorbance of plasmid DNA above 290 nm. Moreover, 10 mM (340 mg/L) of $H_2O_2$ had negligible effect on *amp*$^R$ segment (Figure S1). Thus, $UV_{>290}/H_2O_2$ was applied to investigate the influence of •OH on the degradation of e-ARG. The •OH exposure, $\int[\bullet OH]dt$, in the $UV_{>290}/H_2O_2$ system was obtained by following the degradation of *p*CBA, which was additionally added in the experimental solution. No $UV_{>290}$ direct photolysis of *p*CBA was observed in the absence of $H_2O_2$ (Figure S6). Thus, the •OH exposure was calculated from $\int[^{\cdot}OH]\,dt = -\frac{ln\frac{[pCBA]}{[pCBA]_0}}{k_{\bullet OH,pCBA}}$ (Elovitz and von Gunten 1999), where the $k_{\bullet OH,pCBA}$ is the second-order rate constant of •OH with *p*CBA ($5\times10^9$ $M^{-1}$ $s^{-1}$) (Buxton, Greenstock et al. 1988). The logarithmic-scale degradation of *amp*$^R$ segments exhibited linear correlations with •OH exposure during $UV_{>290}/H_2O_2$ (Figure 1b). The resulting bimolecular rate constants derived from the slopes of linear curves, $k_{\bullet OH,Amp}$ = 2.303 × slope, are summarized in Table 1.

The $k_{\bullet OH,Amp}$ of *amp*$^R$ segments increased with amplicon size, ranging from $8.1\times10^9$ $M^{-1}$ $s^{-1}$ for the 192 bp amplicon to $5.6\times10^{10}$ $M^{-1}$ $s^{-1}$ for the 851 bp amplicon (Table 1). A good linear relationship ($r^2$=0.996) was observed between the $k_{\bullet OH,Amp}$ and the base pair number of *amp*$^R$ segments (Figure S7), which was consistent with previous findings that •OH non-selectively reacts with all nucleotides in a DNA sequence (both AT and GC contents) (He, Zhou et al. 2019). The $k_{\bullet OH,plasmid}$ of the entire plasmid was predicted to be $1.8\times10^{11}$ $M^{-1}$ $s^{-1}$ by applying the base pair number of pUC19 (2686 bps) into the regression equation of this linear curve (Figure S7). Alternatively, similar to the $k_{UV,plasmid}$ as mentioned above, the $k_{\bullet OH,plasmid}$ of

pUC19 was also estimated by normalizing the $k_{\bullet OH,Amp}$ of each segment (qPCR analyses) to the entire plasmid and calculating the average value as $1.5(\pm0.07)\times10^{11}$ $M^{-1}$ $s^{-1}$ (Table 1).

The $k_{\bullet OH,Amp}$ values for the plasmid-encoded $amp^R$ segments in this study were lower by a factor of ~3 than those reported for the chromosome-encoded *blt* genes with similar amplicon length (He, Zhou et al. 2019). To see whether the reactivity difference is due to the conformational difference between the supercoiled-form plasmid and linear-form genomic DNA, the theoretical diffusion-controlled rate constant for the reaction of •OH with supercoiled pUC19 was calculated based on a method proposed by He, Zhou et al. (2019). The theoretical maximum $k_{\bullet OH}$ value was predicted as $3.84\times10^{11}$ $M^{-1}$ $s^{-1}$ for pUC19, which yields a bp-specific $k_{\bullet OH}$ value of $1.43\times10^{8}$ $M_{AT+GC}^{-1}$ $s^{-1}$ when normalized to the length (in AT+GC bps) of pUC19 (2686 bps) (Text S2). For comparison, the theoretical maximum $k_{\bullet OH}$ value was $7.97\times10^{12}$ $M^{-1}$ $s^{-1}$ for a hypothetical 50-kbp linear-form segment of genomic DNA, yielding a bp-specific $k_{\bullet OH}$ value of $1.59\times10^{8}$ $M_{AT+GC}^{-1}$ $s^{-1}$ (He, Zhou et al. 2019). This indicates that the conformational difference between the plasmid (supercoiled) and genomic (linear) DNA (the bp-specific $k_{\bullet OH}$ differed only by a factor of 1.1) does not explain the observed •OH reactivity difference. The maximum $k_{\bullet OH}$ values for the $amp^R$ amplicons can also be calculated by multiplying the bp-specific $k_{\bullet OH}$ ($1.43\times10^{8}$ $M_{AT+GC}^{-1}$ $s^{-1}$) with the length of each amplicon, and ranged from $2.57\times10^{10}$ $M^{-1}$ $s^{-1}$ for 192 bp to $1.14\times10^{11}$ $M^{-1}$ $s^{-1}$ for 851 bp (Text S2). Thus, the experimental $k_{\bullet OH,Amp}$ for pUC19 were lower by a factor of 2.5 than the theoretical maximum $k_{\bullet OH,Amp}$ values. This difference is acceptable considering all possible experimental errors as well as the hypothesis applied in the theoretical calculation.

*Structural degradation of plasmid (Figure 2).* Figure 2a shows the electrophoresis gel of pUC19 exposed to $UV_{254}$. The intact pUC19 before the $UV_{254}$ exposure showed a band located lower than the linearized pUC19 by *EcoRI*. Plasmid DNA generally exists in a supercoiled form,

which is smaller than its linear form and migrates faster in electrophoresis gel. The $UV_{254}$ irradiation (0–130 mJ/cm$^2$) did not change the position of the band, suggesting that the pUC19 kept its supercoiled form without significant conformational change (e.g., strand breakage). It is well documented that the genome damage by $UV_{254}$ is mainly caused by the formation of DNA lesions such as CPDs and 6,4-photoproducts (pyrimidine adducts) (Sinha and Häder 2002, Cadet and Douki 2018), which are generally not detectable by gel electrophoresis analysis (Yoon, Dodd et al. 2018).

The reaction pathways of •OH with DNA include addition to nucleobases – producing adduct radicals – and hydrogen-abstraction from 2-deoxyribose (sugar moiety) (von Sonntag 2006, Dizdaroglu and Jaruga 2012), resulting in not only oxidized bases and abasic sites, but also strand breaks (Cadet, Delatour et al. 1999, von Sonntag 2006). The double-strand breaks are expected to be mainly responsible for the conformational change from supercoiled to linear plasmid form. Gel electrophoresis analysis showed that the pUC19 plasmid band gradually moved from the supercoiled to linear form position with increasing •OH exposure (Figure 2b), revealing the formation of double-strand breaks in pUC19.

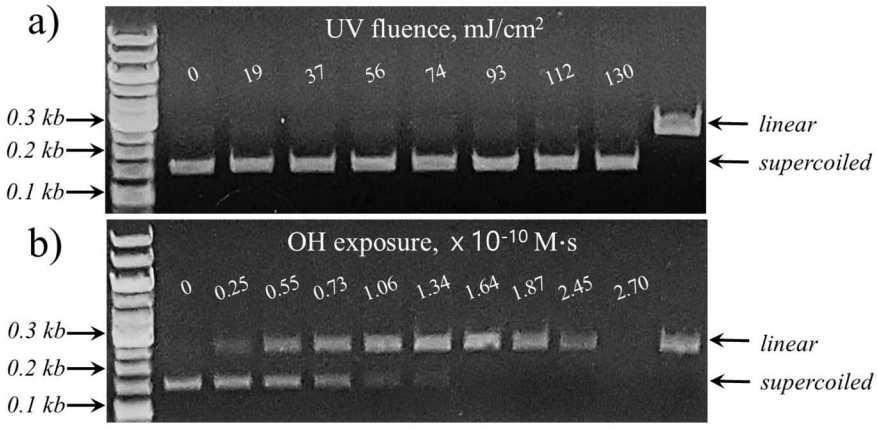


**Figure 2.** DNA electrophoresis gel of pUC19 treated by (a) $UV_{254}$ and (b) •OH ($UV_{>290}/H_2O_2$). First column shows the standard DNA ladders. Last column shows the linearized pUC19 after treating with *EcoRI* restriction digestion.

### 3.2 e-ARG deactivation (loss of transforming activity) during separate exposure to $UV_{254}$ and •OH

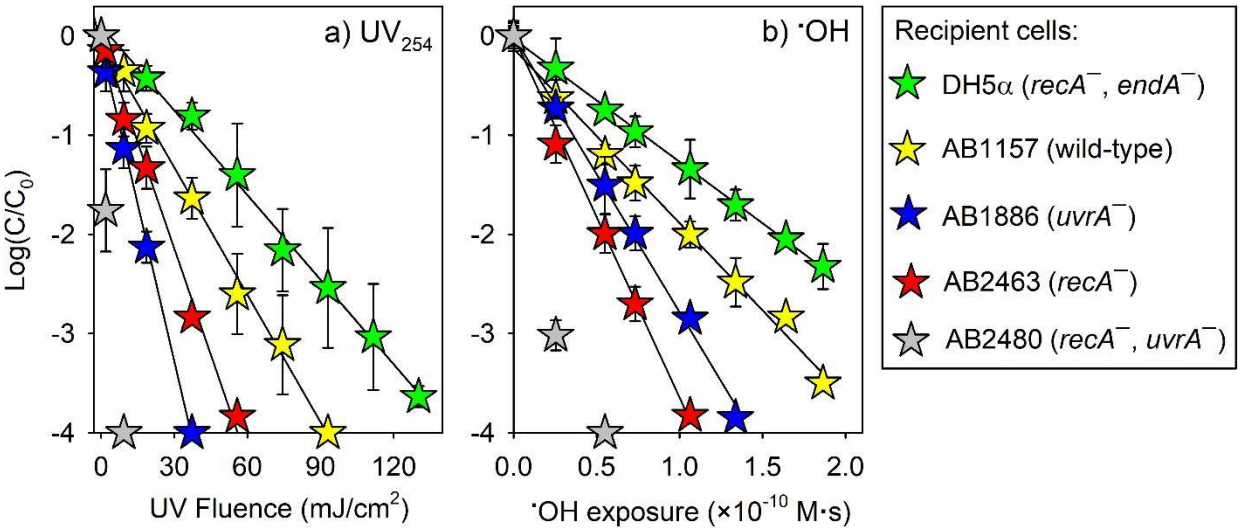


**Figure 3.** Elimination of gene transforming activity during the treatment of pUC19 (1 µg/mL) with (a) $UV_{254}$ and (b) •OH ($UV_{>290}/H_2O_2$) at pH 7 (2 mM phosphate buffer). 10 mM of $H_2O_2$ and 1 µM of *p*CBA were added in $UV_{>290}/H_2O_2$ experiments. The parentheses in legend show the deficient DNA repair genes in recipient cells. Error bars represent the standard deviations of triplicate experiments. Lines are the linear regressions of the experimental data.

Bacterial cells have developed the ability of repairing DNA lesions induced by UV irradiation and oxidant stress (e.g., radicals) using several enzyme systems (Teebor, Boorstein et al. 1988, Sinha and Häder 2002). The biological deactivation of pUC19 upon separate treatment with $UV_{254}$ and •OH was studied by analysing its transformation of non-resistant recipient cells having different DNA repair abilities. The decrease of transforming activity of pUC19 followed first-order kinetics with respect to UV fluence or •OH exposure, and was variable depending on the recipient cells used (Figure 3). The most rapid decrease was observed for AB2480 (*uvrA*$^-$, *recA*$^-$) during each separate treatment with $UV_{254}$ and •OH. No transformant was detectable from AB2480 (more than 4-log decrease) when the UV fluence was above 5 mJ/cm$^2$, or when

387 the •OH exposure was higher than $5.5\times10^{-11}$ M·s. Thus, the fluence-based rate constant for UV
388 ($k_{UV,transformation}$) and second-order rate constant for •OH ($k_{\bullet OH,transformation}$) for the
389 transforming activity loss for AB2480 were not calculated in this case due to the limited data
390 points.

391 During $UV_{254}$ exposure (Figure 3a), the loss of transforming activity was slower in AB1886
392 (*uvrA*$^-$, 0.24 cm$^2$/mJ) than AB2480, followed by AB2463 (*recA*$^-$, 0.16 cm$^2$/mJ), AB1157 (wild-
393 type, 0.10 cm$^2$/mJ), and DH5α (*recA*$^-$, *endA*$^-$, 0.07 cm$^2$/mJ), in which the values in parentheses
394 show $k_{UV,transformation}$ (Table 1). The variation in the transformation efficiency of plasmids
395 carrying the same DNA damage indicated that the UV-induced damage can be repaired by
396 recipient cells to different extents, depending on their repair gene proficiencies (or deficiencies).
397 The *uvrABC* proteins involve the nucleotide excision repair of a variety of DNA lesions
398 including the UV-induced CPDs and 6,4-photoproducts. This process is initiated by the
399 interaction of *uvrA* protein with DNA to recognize the damaged sites (Kisker, Kuper et al.
400 2013). The *recA* protein is essential for the post-replication repair of double-strand breaks and
401 single-strand gaps (e.g., T-T dimers) by homologous recombination (Smith and Wang 1989,
402 Shinohara and Ogawa 1995). These roles of *uvrA and recA* proteins well explained the trend
403 observed from the transformation rates of *E. coli* strains. AB2480 was most sensitive to UV-
404 induced DNA damage on pUC19 due to lack of both *uvrA* and *recA* genes. The *uvrA* deficient
405 AB1886 was the second most sensitive, followed by the *recA* deficient AB2463, indicating that
406 *uvrA* played a more important role than *recA* for the repair of UV-induced DNA damage. The
407 wild-type AB1157 was less sensitive than the other three *E. coli* mutant strains owing to its
408 DNA repair capability by *uvrA* and *recA*. Interestingly, despite its deficiency in *recA*, the DH5α
409 strain exhibited even lower sensitivity to UV-induced DNA damage compared to wild-type
410 AB1157. This was possibly attributable to the lack of a functional *endA* gene in DH5α. The
411 *endA* gene is associated with the formation of extracellular DNase I, which can hydrolyze

412 exogenous plasmid DNA, consequently reducing its uptake and transformation (Shou, Kang et
413 al. 2019). In line with this, the DH5α showed ~10-fold higher transformation efficiency than the
414 other *E. coli* strains proficient in *endA* when all were transformed with equivalent concentrations
415 of undamaged pUC19 (Figure S4). This *endA* deficiency might therefore render *E. coli* DH5α
416 inherently more active for DNA damage repair than the other strains, despite its lack of *recA*.
417 During •OH exposure (Figure 3b), the rate of transforming activity loss was the highest for
418 AB2480 followed by AB2463 (*recA*$^-$, $8.2\times10^{10}$ $M^{-1}$ $s^{-1}$), AB1886 (*uvrA*$^-$, $6.5\times10^{10}$ $M^{-1}$ $s^{-1}$),
419 AB1157 (wild-type, $4.1\times10^{10}$ $M^{-1}$ $s^{-1}$), and DH5α (*recA*$^-$, *endA*$^-$, $2.9\times10^{10}$ $M^{-1}$ $s^{-1}$) in which the
420 values in parentheses show $k_{\bullet OH,transformation}$ (Table 1). The *recA* deficient AB2463 showed
421 higher sensitivity to •OH-induced DNA damage than the *uvrA* deficient AB1886, which was
422 opposite compared to the case for $UV_{254}$ (Figure 3a). This suggests that *recA* is more efficient
423 for repairing •OH-induced DNA damage, as homologous recombination is based on exchange of
424 (damaged) nucleotide sequences (Alberts, Johnson et al. 2002) and capable of repairing not only
425 base oxidation but also double-strand breaks. In contrast, *uvrA* is based on nucleotide excision
426 repair and more specific to the repair of UV-induced DNA lesions (base modification such as
427 CPDs), but not efficient for double-strand breaks (Alberts, Johnson et al. 2002).

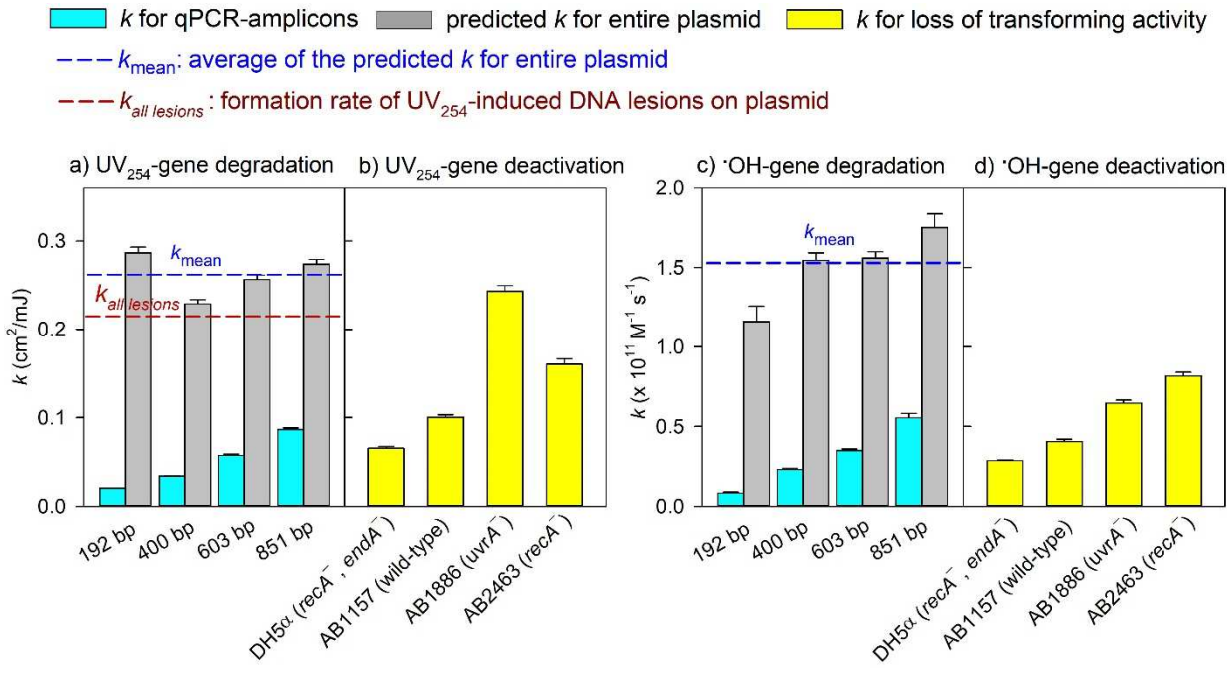


428

429 **Figure 4**. Apparent rate constants for the degradation of *amp*$^R$ segments, pUC19 plasmid, and
430 the elimination of gene transforming activity during exposure to (a, b) $UV_{254}$ and (c, d) •OH
431 ($UV_{>290}/H_2O_2$). Specific kinetic parameters are summarized in Table 1 and error bars represent
432 the standard errors of apparent rate constants. Rate constants for the loss of transforming activity
433 in AB2480 were not calculated due to the limited data points.

434 The apparent rate constants for the degradation of *amp*$^R$ segments, pUC19 plasmid, and the
435 loss of gene transforming activity are compared in Figure 4. For both $UV_{254}$ direct photolysis
436 and •OH oxidation, the estimated degradation rates of the entire plasmid (based on qPCR
437 analyses) overestimated the rates of pUC19 deactivation (loss of transforming activity) observed
438 for all repair-proficient *E. coli* recipient strains, which can be explained by the repair of $UV_{254}$-
439 and •OH-induced damage by repair-proficient recipient cells. Our results were in agreement
440 with previous findings on the $UV_{254}$ treated pWH1266 plasmid and its transformation of
441 *Acinetobacter baylyi* (Chang, Juhrend et al. 2017). However, the rate of gene deactivation
442 during $UV_{254}$ direct photolysis measured using *uvrA* deficient AB1886 as the recipient strain
443 was close to the estimated degradation rate of pUC19 and the formation rate of DNA lesions

(Figure 4a, b). The minimum rates of gene deactivation measured by double mutant AB2480 (*uvrA*$^-$, *recA*$^-$) were estimated based on the limited data points shown in Figure 3, which gave 0.91 cm$^2$/mJ and 1.7×10$^{11}$ M$^{-1}$ s$^{-1}$ for $UV_{254}$ and •OH exposure, respectively. These values were significantly larger than the gene deactivation rates measured by any of the repair proficient strains. Furthermore, the degradation rate of the entire plasmid underestimated the loss of pUC19 transforming activity measured by AB2480 (*uvrA*$^-$, *recA*$^-$) during $UV_{254}$ direct photolysis and •OH oxidation.

### 3.3 e-ARG degradation and deactivation by combined exposure to $UV_{254}$ and radicals

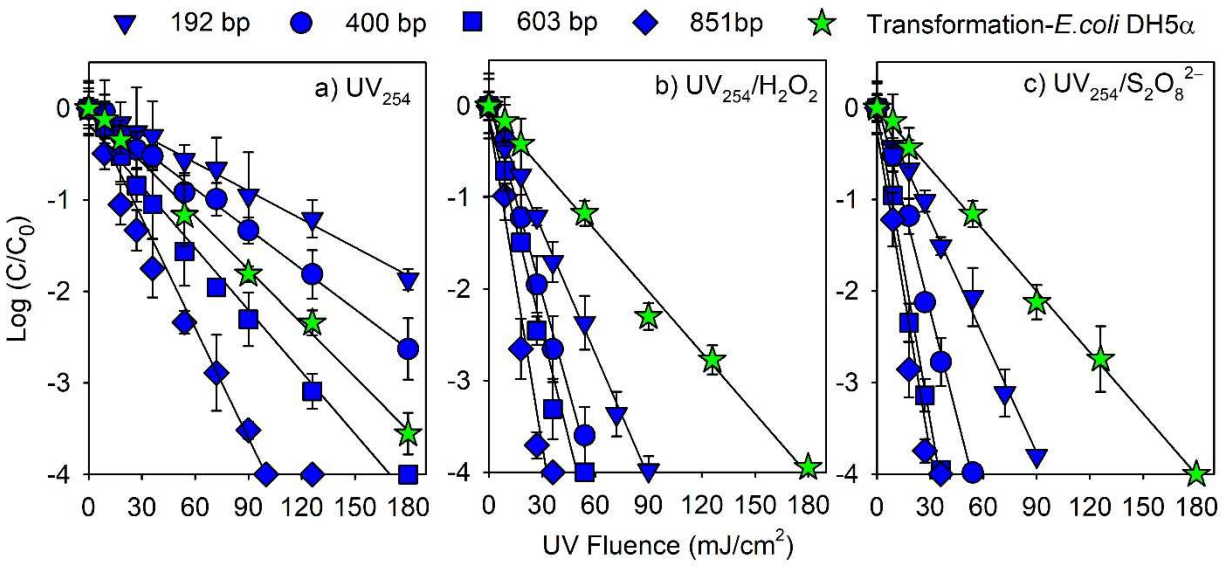


**Figure 5**. Degradation of *amp*$^R$ segments and elimination of gene transforming activity (*E.coli* DH5α as recipient cells) with increasing UV fluence (0–180 mJ/cm$^2$) during treatment of pUC19 (0.3 μg/mL) with (a) $UV_{254}$, (b) $UV_{254}/H_2O_2$ (0.5 mM), and (c) $UV_{254}/S_2O_8^{2-}$ (0.5 mM) at pH 7 (2 mM phosphate buffer). *p*CBA (1 μM) was added in $UV_{254}/H_2O_2$ experiments for the quantification of •OH, and both *p*CBA and nitrobenzene (each 1 μM) were added in $UV/S_2O_8^{2-}$ experiments for the quantification of •OH and $SO_4^{\bullet-}$. Error bars represent the standard deviations of triplicate experiments. Lines represent the linear regressions of experimental data.

460 The degradation of *amp*$^R$ and the elimination of gene transforming activity (*E. coli* DH5α as
461 recipient cells) were tested during combined exposure to $UV_{254}$ and radicals (•OH and $SO_4^{\bullet-}$), in
462 comparison to $UV_{254}$ direct photolysis. The degradation of *amp*$^R$ amplicons followed first-order
463 kinetics with respect to UV fluence ($r^2$ >0.99) during $UV_{254}$, $UV_{254}/H_2O_2$, and $UV_{254}/S_2O_8^{2-}$
464 treatments (Figure 5). A lower initial concentration of pUC19 (0.3 μg/mL) and a higher fluence
465 range (0–180 mJ/cm$^2$) were applied in these tests than in the experiments described in the
466 preceding sections. However, the degradation rate constants of *amp*$^R$ amplicons upon $UV_{254}$
467 direct photolysis (i.e., $2.4\times10^{-2}$–$8.2\times10^{-2}$ cm$^2$/mJ) (Table S1) were in good agreement with
468 those obtained during the treatment of 1 μg/mL of pUC19 by 0-130 mJ/cm$^2$ of $UV_{254}$ (i.e.,
469 $2.0\times10^{-2}$–$8.9\times10^{-2}$ cm$^2$/mJ, Table 1). The $k_{UV_{254}/H_2O_2}$ of *amp*$^R$ amplicons during $UV_{254}/H_2O_2$
470 were in the range of $1.0\times10^{-1}$–$3.0\times10^{-1}$ cm$^2$/mJ, which were larger than the $k_{UV_{254}}$ by a factor of
471 ~4 (Table S1). Therefore, the contribution of $UV_{254}$ direct photolysis to the overall gene
472 degradation during $UV_{254}/H_2O_2$ was only about 25% ($k_{UV_{254}}/k_{UV_{254}/H_2O_2} \times 100\%$), revealing
473 the significant role of •OH exposure (75%).
474 The $k_{UV_{254}/H_2O_2}$ for the elimination of gene transforming activity was $(5.1\pm0.2)\times10^{-2}$ cm$^2$/mJ,
475 which was larger than the $k_{UV_{254}}$ by a factor of only 1.1 ($k_{UV_{254}/H_2O_2}/k_{UV_{254}} = 1.1$, Table S1).
476 Thus, even though the •OH exposure significantly accelerated gene degradation (by a factor of
477 4), its contribution to the elimination of gene transforming activity was not as efficient as
478 expected.

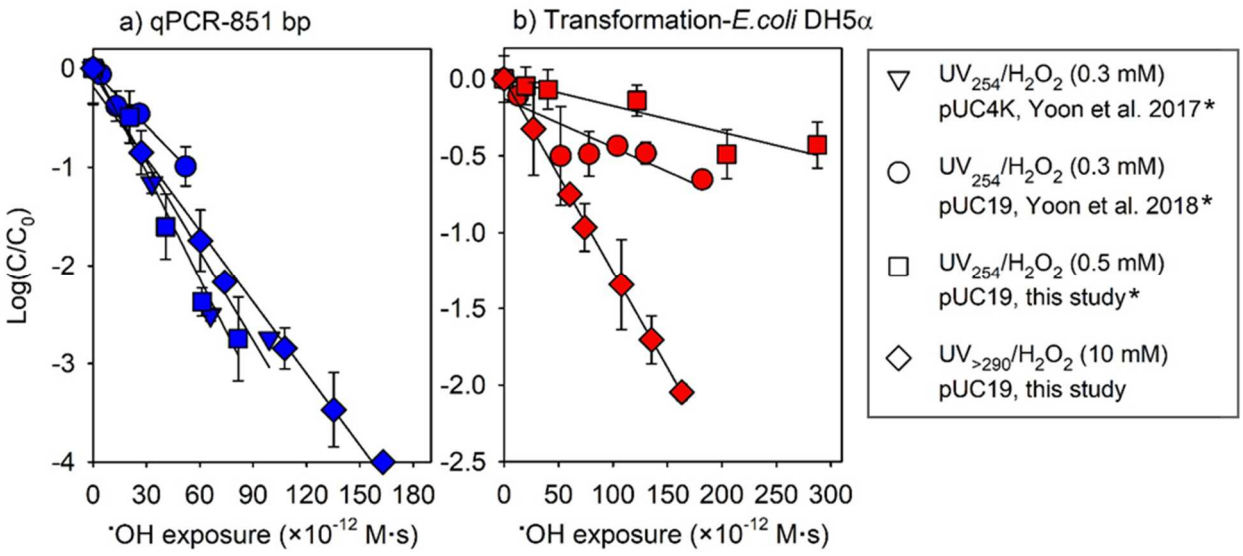


**Figure 6**. (a) Degradation of *amp*$^R$ segment (851 bp) and (b) elimination of gene transforming activity (*E. coli* DH5α as recipient cells) as a function of •OH exposure during UV/$H_2O_2$ treatments at different UV (254 nm and >290 nm) and $H_2O_2$ (0.3 mM, 0.5 mM, and 10 mM) conditions. The gene transforming activity was not measured in the study of Yoon et al. 2017 for treating pUC4k with $UV_{254}/H_2O_2$ (0.3 mM). The values for the data sets designated by (*) represent contributions from •OH exposure only (estimated by subtracting $UV_{254}$ contributions from overall measurements of qPCR signal or transforming activity loss). Error bars represent the standard deviations of triplicate experiments. Lines represent the linear regressions of experimental data.

Figure 6 summarizes the results from this study and the literature on the effect of •OH exposure on degradation of the 851 bp *amp*$^R$ segment and loss of gene transforming activity (measured using *E. coli* DH5α as recipient strain). Plasmid pUC4k or pUC19 carrying *amp*$^R$ was treated with UV/$H_2O_2$ at different conditions of UV wavelength and initial $H_2O_2$ concentrations, i.e., $UV_{254}/H_2O_2$ (0.3 mM or 0.5 mM) and $UV_{>290}/H_2O_2$ (10 mM). The •OH-induced degradation or deactivation were calculated by subtracting the effect of $UV_{254}$ direct photolysis from the overall results of corresponding $UV_{254}/H_2O_2$. Although the statistical analysis showed a significant variation ($p$=0.0149) in the slopes of linear curves in Figure 6a,

497 the $k_{\bullet OH,851\ bp}$ values during $UV_{254}/H_2O_2$ treatment differed only by factors of 0.8−1.5 from that
498 during •OH only process ($UV_{>290}/H_2O_2$). This suggested that $UV_{254}$-induced gene damage on the
499 plasmid (e.g., CPDs and pyrimidine adducts) did not cause significant impact on the reactivity
500 of •OH with nucleobase and sugar moieties during $UV_{254}/H_2O_2$. However, the elimination of
501 gene transforming activity (measured using *E. coli* DH5α as recipient strain) varied significantly
502 in the different treatments. The loss of gene transforming activity was ~5 times slower in
503 $UV_{254}/H_2O_2$ processes ($UV_{254}$ and •OH co-exist) as compared to that obtained from
504 $UV_{>290}/H_2O_2$ (•OH only). This indicates that the elimination of gene transforming activity
505 caused by $UV_{254}$ direct photolysis and •OH oxidation were not additive during $UV_{254}/H_2O_2$. One
506 possible explanation could be that some DNA damage repair pathways such as nucleotide
507 excision repair by *uvr*ABC also repaired •OH-induced lesions (e.g., base oxidation) located near
508 the UV-induced lesions, leading to much less extensive loss of transforming activity than would
509 be expected from simple summation of the losses in transforming activity observed for $UV_{254}$
510 and •OH exposure separately.
511 The degradation rates of $amp^R$ amplicons ($1.0\times10^{-1}$–$3.2\times10^{-1}$ $cm^2/mJ$) during $UV_{254}/ S_2O_8^{2-}$
512 were also ~4-fold larger than that obtained during $UV_{254}$ (Table S1). $SO_4^{\bullet-}$ is the primary radical
513 generated during $UV_{254}$ photolysis of $S_2O_8^{2-}$. However, $SO_4^{\bullet-}$ can further react with $H_2O$, $OH^-$,
514 and $Cl^-$ (sometimes present as an impurity) in aqueous solution to produce •OH (Lutze, Kerlin
515 et al. 2015). Using the degradation kinetics of radical probe compounds (nitrobenzene and
516 *p*CBA) (Figures S7 and S8), the steady-state concentration of •OH during $UV_{254}/S_2O_8^{2-}$ was
517 determined to be $6.4\times10^{-13}$ M, which was approximately two orders of magnitude smaller than
518 that of $SO_4^{\bullet-}$ ($1.8\times10^{-11}$ M) under experimental conditions used here (Text S3). This was
519 consistent with the theoretically estimated values considering all the possible reactions related to
520 •OH formation in $UV_{254}/S_2O_8^{2-}$ system (Text S4). Despite the much lower concentration, the
521 contribution of •OH to the overall gene damage cannot be ignored, as the $amp^R$ segments

appeared to be much more reactive to •OH than $SO_4^{\bullet-}$ (see discussions below). Thus, the percentages of gene degradation attributable to $UV_{254}$ direct photolysis, $SO_4^{\bullet-}$, and •OH during $UV_{254}/S_2O_8^{2-}$ treatment could be estimated as ~23%, ~33%, and ~44%, respectively, in which the relative contributions of each pathway to the overall gene damage were calculated based on the observed rate constants for degradation of $amp^R$ amplicons during $UV_{254}$ and $UV_{254}/S_2O_8^{2-}$treatments, the steady-state concentrations of •OH and $SO_4^{\bullet-}$ in $UV_{254}/S_2O_8^{2-}$ experiments, and the second-order rate constants for reactions of •OH and $SO_4^{\bullet-}$ with the $amp^R$ amplicons (Text S5).

The second-order rate constants of $SO_4^{\bullet-}$ with $amp^R$ segments were determined to be in the range of $(1.07–1.96)\times10^9$ $M^{-1}$ $s^{-1}$ (Text S5 and Table S2), which were about an order of magnitude lower than the •OH rate constants (Table 1). $SO_4^{\bullet-}$ preferentially adds to the electron-rich sites of the nucleobases (e.g., $C_5$ of pyrimidines) to generate radical adducts, which decay to nucleobase radicals as intermediates, followed by hydroxylation and oxidation in aqueous solution (von Sonntag 2006). However, $SO_4^{\bullet-}$ is larger than •OH and negatively charged. Therefore, steric hindrance and electrostatic repulsion might decrease the reactivity of $SO_4^{\bullet-}$ toward negatively charged DNA molecules in comparison to •OH.

Similar to $UV_{254}/H_2O_2$ processes, the elimination rate of pUC19 transforming activity during $UV_{254}/S_2O_8^{2-}$ treatment was also only slightly larger than that in $UV_{254}$ direct photolysis ($k_{UV_{254}/S_2O_8^{2-}}/k_{UV_{254}} = 1.1$, Table S1), even while the observed amplicon *degradation* rates were ~4-fold faster for $UV_{254}/S_2O_8^{2-}$ compared to $UV_{254}$ direct photolysis. This further supports the above findings that co-exposure to $UV_{254}$ and radicals during $UV_{254}$-AOPs did not lead to faster transforming activity loss than the separate exposures to $UV_{254}$ and radicals, due to the facile repair of $UV_{254}$ and/or radical-induced DNA damage in host cells.

### 3.5 Effect of wastewater effluent organic matter on the degradation of *amp*$^R$ during UV$_{254}$-AOPs

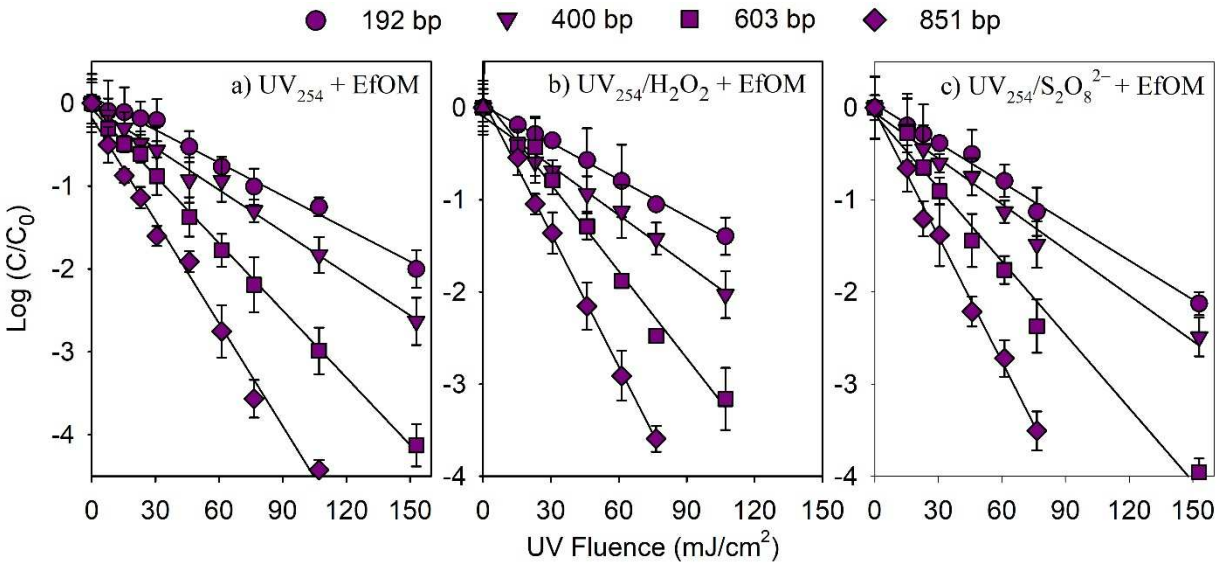


**Figure 7.** Degradation of *amp*$^R$ segments in the presence of wastewater effluent organic matter (5.4 mg C/L) during the treatment of pUC19 (0.31 μg/mL) with (a) $UV_{254}$, (b) $UV_{254}/H_2O_2$ (0.5 mM), and (c) $UV_{254}/S_2O_8^{2-}$ (0.5 mM) at pH 7 (2 mM phosphate buffer). *p*CBA (1 μM) was added in $UV_{254}/H_2O_2$ experiments for the quantification of •OH, and both *p*CBA and nitrobenzene (each 1 μM) were added in $UV/S_2O_8^{2-}$ experiments for the quantification of •OH and $SO_4^{\bullet-}$. Error bars represent the standard deviations of triplicate experiments. Lines represent the linear regressions of experimental data.

The efficiencies of *amp*$^R$ degradation during $UV_{254}$, $UV_{254}/H_2O_2$, and $UV_{254}/S_2O_8^{2-}$ experiments were investigated in the presence of EfOM (5.4 mg C/L). The UV 254 nm absorbance of EfOM solution ($a_{254}$) was 0.1 cm$^{-1}$. The path length in the petri dish (L) was 1.6 cm. Thus, the water factor, $WF=(1-10^{-a254 \cdot L})/(a_{254} \cdot L \cdot \ln 10)$ (Bolton and Linden 2003), was calculated to be 0.84. The average UV intensity in the solution containing EfOM was then corrected from 0.30 mW/cm$^2$ to 0.25 mW/cm$^2$ using the calculated water factor (Lee, Gerrity et al. 2016). The *amp*$^R$ segments were gradually degraded with increasing UV fluence following

562 first-order kinetics (Figure 7). Interestingly, the $k_{UV,Amp}$ of each segment during $UV_{254}$
563 irradiation in the presence of EfOM was approximately 1.2 times higher than the corresponding
564 conditions without EfOM ($p$<0.0001) (Table S1). Chromophoric dissolved organic matter
565 (DOM) is known to generate reactive species upon UV irradiation, such as triplet excited states
566 of DOM ($^3$DOM*), singlet oxygen, and •OH, which have been proven to contribute to the
567 oxidation of organic pollutants (Chin, Miller et al. 2004, Lester, Sharpless et al. 2013, Batista,
568 Teixeira et al. 2016, Rosario-Ortiz and Canonica 2016). Bacteriophage MS2 was found to be
569 inactivated by $^3$DOM* and singlet oxygen generated from sunlight irradiation of wastewater and
570 river water DOM isolates (Kohn, Grandbois et al. 2007, Kohn and Nelson 2007, Rosado-Lausell,
571 Wang et al. 2013). The reactive oxygen species (e.g., singlet oxygen, superoxide, $H_2O_2$)
572 generated during photooxidations involving $^3$DOM* were proposed to inactivate bacteria by
573 damaging DNA, proteins, and cell membranes (Song, Mohseni et al. 2016, Nelson, Boehm et al.
574 2018). Our findings suggest that through its photosensitizing properties, DOM can indirectly
575 contribute to the photodegradation of e-ARGs. Similar results were reported recently on the
576 enhanced photo-degradation of pBR322 plasmid-encoded *tet A* and $bla_{TEM\text{-}1}$ genes in DOM
577 solution (Zhang, Li et al. 2019). This degradation pathway might play an especially important
578 role during solar disinfection processes, due to the low UV absorbance characteristics of DNA at
579 high wavelengths (and consequent minimal direct UV photolysis under such conditions).

580 In contrast, EfOM mainly acted as radical scavenger during $UV_{254}/H_2O_2$ and $UV_{254}/S_2O_8^{2-}$
581 experiments. The $k_{UV_{254}/H_2O_2}$ and $k_{UV_{254}/S_2O_8^{2-}}$ of $amp^R$ segments in the presence of EfOM were
582 each decreased by a factor of ~3 compared to the conditions without EfOM (Table S1). The
583 degradation kinetics of *p*CBA and nitrobenzene (Figure S10) also confirmed the much lower
584 levels of radicals in the presence of EfOM (e.g., $[SO_4^{\bullet-}]_{ss}$: $9.5\times10^{-13}$ M with EfOM *vs.* $1.8\times10^{-11}$
585 M without EfOM). Overall, the degradation efficiency of $amp^R$ in the presence of EfOM

586 increased only marginally (within a factor of 1.4) during $UV_{254}/H_2O_2$ and $UV_{254}/S_2O_8^{2-}$,

587 compared to $UV_{254}$ alone, due to the significant scavenging of radicals by EfOM.

## 4. Conclusions

- The degradation of *amp*$^R$ segments and the loss of gene transforming activity followed first-order kinetics with respect to UV fluence and •OH exposure during $UV_{254}$ direct photolysis and •OH oxidation ($UV_{>290}/H_2O_2$). The degradation rate constants of *amp*$^R$ segments increased with amplicon size, which corresponded to the increase in nucleotide bps (and hence, reaction sites) with increased amplicon length. Gel electrophoresis results indicated that $UV_{254}$ (0–130 mJ/cm$^2$) did not change the supercoiled conformation of pUC19 plasmid, whereas •OH exposure (0–$2.7\times10^{-10}$ M·s) led to strand-breaks.
- The loss of gene transforming activity varied depending on the type of recipient cells. Double mutant AB2480, which was deficient in repair genes *uvrA* and *recA*, was the most sensitive to DNA damage induced by $UV_{254}$ direct photolysis and •OH oxidation. The predicted degradation rates for the entire pUC19 plasmid overestimated the loss in transforming activity of pUC19 for all recipient cells other than AB2480, apparently due to the repair of DNA damage by repair-proficient strains.
- The second-order rate constants of •OH with *amp*$^R$ segments were determined to be in the range of $8.1\times10^9$ – $5.6\times10^{10}$ ($M^{-1}$ $s^{-1}$) and showed a strong linear relationship with the base pair number of *amp*$^R$ segments, suggesting that •OH reacts with all nucleobases of plasmid DNA non-selectively. The rate constants of $SO_4^{\bullet-}$ with *amp*$^R$ segments were an order of magnitude lower than the corresponding •OH rate constants; thus, the contribution of the trace amount of •OH to the overall gene damage cannot be ignored during $UV_{254}/S_2O_8^{2-}$ treatment.
- Although •OH and $SO_4^{\bullet-}$ significantly accelerated (~75%) the degradation of *amp*$^R$ amplicons measured by qPCR during $UV_{254}/H_2O_2$ and $UV_{254}/S_2O_8^{2-}$ experiments, this only marginally increased the gene deactivation rate (~11%), as gene damage caused by $UV_{254}$ and radical co-exposure appeared to be repaired more efficiently by recipient cells than the

gene damage from the separate $UV_{254}$ and radical exposures. Thus, the elimination efficiency of the ARGs' transforming activities was similar for $UV_{254}$ vs $UV_{254}$-AOPs at the same UV fluence, and the extent of elimination was mainly determined by the level of UV fluence. Because the transforming activity of the $amp^R$ gene could be lowered by only ~1-log at a typical UV disinfection fluence for water treatment (e.g., 40 mJ/cm$^2$) but increased to more than 4-logs at an elevated UV fluence for UV-AOPs (e.g., 500 mJ/cm$^2$), the use of UV-AOPs may still prove beneficial for ARG degradation and deactivation, with the accompanying benefit of improved degradation of trace organic contaminants.

- Reactive species formed from the excitation of chromophoric organic matter appear to contribute to accelerated degradation of $amp^R$ during $UV_{254}$ irradiation in the presence of EfOM (compared to direct photolysis by $UV_{254}$ alone), whereas EfOM mainly acted as a radical scavenger in $UV_{254}/H_2O_2$ and $UV_{254}/S_2O_8^{2-}$ experiments.

## Acknowledgements

This study was supported by the Korea Institute of Marine Science & Technology Promotion funded by the National Research Foundation funded by the Ministry of Science, ICT and Future Planning (NRF-2020R1A2C2011951). Curtin University (Curtin International Postgraduate Research Scholarship) and Water Research Australia (WaterRA Postgraduate Scholarship) are gratefully acknowledged for providing financial support for M. Nihemaiti. Additional support for H. He and M. C. Dodd from U.S. National Science Foundation Grant Number CBET-1254929 is gratefully acknowledged.

# Reference


Alberts, B., et al. (2002). Molecular Biology of the Cell, 4th edition. New York, Garland Science.

Batista, A. P. S., et al. (2016). "Correlating the chemical and spectroscopic characteristics of natural organic matter with the photodegradation of sulfamerazine." Water Research **93**: 20-29.

Bioneer (2016). "AccuPrep® Nano-Plus Plasmid Mini/Midi/Maxi Extraction Kit." User's Guide **Available at http://us.bioneer.com/Protocol/AccuPrep%20Nano-Plus%20Plasmid%20Extraction%20Kit.pdf**.

Bolton, J. R. and K. G. Linden (2003). "Standardization of methods for fluence (UV Dose) determination in bench-scale UV experiments." Journal of Environmental Engineering **129**(3): 209-215.

Buxton, G. V., et al. (1988). "Critical Review of rate constants for reactions of hydrated electrons, hydrogen atoms and hydroxyl radicals ($\cdot$OH/$\cdot$O$^-$) in Aqueous Solution." Journal of Physical and Chemical Reference Data **17**(2): 513-886.

Cacace, D., et al. (2019). "Antibiotic resistance genes in treated wastewater and in the receiving water bodies: A pan-European survey of urban settings." Water Research **162**: 320-330.

Cadet, J., et al. (1999). "Hydroxyl radicals and DNA base damage." Mutation Research/Fundamental and Molecular Mechanisms of Mutagenesis **424**(1): 9-21.

Cadet, J. and T. Douki (2018). "Formation of UV-induced DNA damage contributing to skin cancer development." Photochemical & Photobiological Sciences **17**(12): 1816-1841.

Chang, P. H., et al. (2017). "Degradation of Extracellular Antibiotic Resistance Genes with UV254 Treatment." Environmental Science & Technology **51**(11): 6185-6192.

Chin, Y.-P., et al. (2004). "Photosensitized Degradation of Bisphenol A by Dissolved Organic Matter." Environmental Science & Technology **38**(22): 5888-5894.

Christou, A., et al. (2017). "The potential implications of reclaimed wastewater reuse for irrigation on the agricultural environment: The knowns and unknowns of the fate of antibiotics and antibiotic resistant bacteria and resistance genes – A review." Water Research **123**: 448-467.

Davies, J. and D. Davies (2010). "Origins and Evolution of Antibiotic Resistance." Microbiology and Molecular Biology Reviews : MMBR **74**(3): 417-433.

675 Dizdaroglu, M. and P. Jaruga (2012). "Mechanisms of free radical-induced damage to DNA."
676 Free Radical Research **46**(4): 382-419.

677
678 Dodd, M. C. (2012). "Potential impacts of disinfection processes on elimination and
679 deactivation of antibiotic resistance genes during water and wastewater treatment." Journal of
680 Environmental Monitoring **14**(7): 1754-1771.

681
682 Elovitz, M. S. and U. von Gunten (1999). "Hydroxyl Radical/Ozone Ratios During Ozonation
683 Processes. I. The Rct Concept." Ozone: Science & Engineering **21**(3): 239-260.

684
685 Ferro, G., et al. (2016). "Antibiotic resistance spread potential in urban wastewater effluents
686 disinfected by UV/H2O2 process." Science of the Total Environment **560-561**: 29-35.

687
688 Ferro, G., et al. (2017). "β-lactams resistance gene quantification in an antibiotic resistant
689 Escherichia coli water suspension treated by advanced oxidation with UV/H2O2." Journal of
690 Hazardous Materials **323**: 426-433.

691
692 Giannakis, S., et al. (2018). "Solar photo-Fenton disinfection of 11 antibiotic-resistant bacteria
693 (ARB) and elimination of representative AR genes. Evidence that antibiotic resistance does not
694 imply resistance to oxidative treatment." Water Research **143**: 334-345.

695
696 Görner, H. (1994). "New trends in photobiology: Photochemistry of DNA and related
697 biomolecules: Quantum yields and consequences of photoionization." Journal of Photochemistry
698 and Photobiology B: Biology **26**(2): 117-139.

699
700 Guo, M.-T., et al. (2015). "Distinguishing Effects of Ultraviolet Exposure and Chlorination on
701 the Horizontal Transfer of Antibiotic Resistance Genes in Municipal Wastewater."
702 Environmental Science & Technology **49**(9): 5771-5778.

703
704 He, H., et al. (2019). "Degradation and Deactivation of Bacterial Antibiotic Resistance Genes
705 during Exposure to Free Chlorine, Monochloramine, Chlorine Dioxide, Ozone, Ultraviolet Light,
706 and Hydroxyl Radical." Environmental Science & Technology **53**(4): 2013-2026.

707
708 Hiller, C. X., et al. (2019). "Antibiotic microbial resistance (AMR) removal efficiencies by
709 conventional and advanced wastewater treatment processes: A review." Science of the Total
710 Environment **685**: 596-608.

711
712 Hong, P.-Y., et al. (2018). "Reusing Treated Wastewater: Consideration of the Safety Aspects
713 Associated with Antibiotic-Resistant Bacteria and Antibiotic Resistance Genes." Water **10**(3).

714
715 Kisker, C., et al. (2013). "Prokaryotic Nucleotide Excision Repair." **5**(3): a012591-a012591.

716

717 Kohn, T., et al. (2007). "Association with Natural Organic Matter Enhances the Sunlight-
718 Mediated Inactivation of MS2 Coliphage by Singlet Oxygen." Environmental Science &
719 Technology **41**(13): 4626-4632.

720
721 Kohn, T. and K. L. Nelson (2007). "Sunlight-Mediated Inactivation of MS2 Coliphage via
722 Exogenous Singlet Oxygen Produced by Sensitizers in Natural Waters." Environmental Science
723 & Technology **41**(1): 192-197.

724
725 Lee, Y., et al. (2016). "Organic Contaminant Abatement in Reclaimed Water by UV/H2O2 and
726 a Combined Process Consisting of O3/H2O2 Followed by UV/H2O2: Prediction of Abatement
727 Efficiency, Energy Consumption, and Byproduct Formation." Environmental Science &
728 Technology **50**(7): 3809-3819.

729
730 Lester, Y., et al. (2013). "Production of Photo-oxidants by Dissolved Organic Matter During UV
731 Water Treatment." Environmental Science & Technology **47**(20): 11726-11733.

732
733 Liu, S.-S., et al. (2018). "Chlorine disinfection increases both intracellular and extracellular
734 antibiotic resistance genes in a full-scale wastewater treatment plant." Water Research **136**: 131-
735 136.

736
737 Lorenz, M. G. and W. Wackernagel (1994). "Bacterial gene transfer by natural genetic
738 transformation in the environment." Microbiological Reviews **58**(3): 563-602.

739
740 Lorenz, M. G. and W. Wackernagel (1994). "Bacterial gene transfer by natural genetic
741 transformation in the environment." Microbiol. Mol. Biol. Rev. **58**(3): 563-602.

742
743 Luby, E., et al. (2016). "Molecular Methods for Assessment of Antibiotic Resistance in
744 Agricultural Ecosystems: Prospects and Challenges." Journal of Environment Quality **45**(2): 441.

745
746 Lutze, H. V., et al. (2015). "Sulfate radical-based water treatment in presence of chloride:
747 Formation of chlorate, inter-conversion of sulfate radicals into hydroxyl radicals and influence
748 of bicarbonate." Water Research **72**: 349-360.

749
750 Mao, D., et al. (2014). "Persistence of Extracellular DNA in River Sediment Facilitates
751 Antibiotic Resistance Gene Propagation." Environmental Science & Technology **48**(1): 71-78.

752
753 McKinney, C. W. and A. Pruden (2012). "Ultraviolet disinfection of antibiotic resistant bacteria
754 and their antibiotic resistance genes in water and wastewater." Environmental Science and
755 Technology **46**(24): 13393-13400.

756
757 Michael-Kordatou, I., et al. (2015). "Erythromycin oxidation and ERY-resistant Escherichia coli
758 inactivation in urban wastewater by sulfate radical-based oxidation process under UV-C
759 irradiation." Water Research **85**: 346-358.

Nagler, M., et al. (2018). "Extracellular DNA in natural environments: features, relevance and applications." Applied Microbiology and Biotechnology **102**(15): 6343-6356.

Nelson, K. L., et al. (2018). "Sunlight-mediated inactivation of health-relevant microorganisms in water: a review of mechanisms and modeling approaches." Environmental Science: Processes & Impacts **20**(8): 1089-1122.

Neta, P., et al. (1988). "Rate Constants for Reactions of Inorganic Radicals in Aqueous Solution." Journal of Physical and Chemical Reference Data **17**(3): 1027-1284.

Neta, P., et al. (1977). "Rate constants and mechanism of reaction of SO4·- with aromatic compounds." Journal of the American Chemical Society **99**(1): 163-164.

Osińska, A., et al. (2020). "Small-scale wastewater treatment plants as a source of the dissemination of antibiotic resistance genes in the aquatic environment." Journal of Hazardous Materials **381**: 121221.

Pruden, A. (2014). "Balancing Water Sustainability and Public Health Goals in the Face of Growing Concerns about Antibiotic Resistance." Environmental Science & Technology **48**(1): 5-14.

Rosado-Lausell, S. L., et al. (2013). "Roles of singlet oxygen and triplet excited state of dissolved organic matter formed by different organic matters in bacteriophage MS2 inactivation." Water Research **47**(14): 4869-4879.

Rosario-Ortiz, F. L. and S. Canonica (2016). "Probe Compounds to Assess the Photochemical Activity of Dissolved Organic Matter." Environmental Science & Technology **50**(23): 12532-12547.

Shanehbandi, D., et al. (2013). "Vibration and glycerol-mediated plasmid DNA transformation for Escherichia coli." FEMS Microbiology Letters **348**(1): 74-78.

Shinohara, A. and T. Ogawa (1995). "Homologous recombination and the roles of double-strand breaks." Trends in Biochemical Sciences **20**(10): 387-391.

Shou, W., et al. (2019). "Substituted Aromatic-Facilitated Dissemination of Mobile Antibiotic Resistance Genes via an Antihydrolysis Mechanism Across an Extracellular Polymeric Substance Permeable Barrier." Environmental Science & Technology **53**(2): 604-613.

Sinha, R. P. and D.-P. Häder (2002). "UV-induced DNA damage and repair: a review." Photochemical & Photobiological Sciences **1**(4): 225-236.

Smith, K. C. and T.-C. V. Wang (1989). "recA-dependent DNA repair processes." BioEssays **10**(1): 12-16.

Song, K., et al. (2016). "Application of ultraviolet light-emitting diodes (UV-LEDs) for water disinfection: A review." Water Research **94**: 341-349.

Stefan, M. I. (2018). Advanced Oxidation Processes for Water Treatment. Fundamentals and Applications, IWA Publishing.

Teebor, G. W., et al. (1988). "The Repairability of Oxidative Free Radical Mediated Damage to DNA: A Review." International Journal of Radiation Biology **54**(2): 131-150.

Vikesland, P. J., et al. (2017). "Toward a Comprehensive Strategy to Mitigate Dissemination of Environmental Sources of Antibiotic Resistance." Environmental Science & Technology **51**(22): 13061-13069.

von Sonntag, C. (2006). Free-radical-induced DNA damage and its repair: A chemical perspective. Heidelberg, Berlin, Springer.

Wu, D., et al. (2019). "Urban and agriculturally influenced water contribute differently to the spread of antibiotic resistance genes in a mega-city river network." Water Research **158**: 11-21.

Yoon, Y., et al. (2017). "Inactivation efficiency of plasmid-encoded antibiotic resistance genes during water treatment with chlorine, UV, and UV/H2O2." Water Research **123**: 783-793.

Yoon, Y., et al. (2018). "Elimination of transforming activity and gene degradation during UV and UV/H2O2 treatment of plasmid-encoded antibiotic resistance genes." Environmental Science: Water Research & Technology.

Zhang, T., et al. (2019). "Removal of antibiotic resistance genes and control of horizontal transfer risk by UV, chlorination and UV/chlorination treatments of drinking water." Chemical Engineering Journal **358**: 589-597.

Zhang, X., et al. (2019). "Enhanced Photodegradation of Extracellular Antibiotic Resistance Genes by Dissolved Organic Matter Photosensitization." Environmental Science & Technology **53**(18): 10732-10740.

Zhang, Y., et al. (2017). "Subinhibitory Concentrations of Disinfectants Promote the Horizontal Transfer of Multidrug Resistance Genes within and across Genera." Environmental Science & Technology **51**(1): 570-580.

Zhang, Y., et al. (2018). "Cell-free DNA: A Neglected Source for Antibiotic Resistance Genes Spreading from WWTPs." Environmental Science & Technology **52**(1): 248-257.

Zheng, J., et al. (2017). "Effects and mechanisms of ultraviolet, chlorination, and ozone disinfection on antibiotic resistance genes in secondary effluents of municipal wastewater treatment plants." Chemical Engineering Journal **317**: 309-316.

Zheng, X., et al. (2014). "Contribution of effluent organic matter (EfOM) to ultrafiltration (UF) membrane fouling: Isolation, characterization, and fouling effect of EfOM fractions." Water Research **65**: 414-424.

## Graphical Abstract